^{1}H NMR Relaxation Studies of the Hydrogen-Bonded Imino Protons of Poly(dA-dT)†

Nuria Assa-Munt,‡ Joseph Granot,§ Ronald W. Behling, and David R. Kearns*

ABSTRACT: Measurements on the thymine imino proton relaxation rates have been used to study various structural and dynamic properties of 53 ± 15 base pair long poly(dA-dT). Below 10 °C, the relaxation is dominated by dipolar magnetic interactions. At 1 °C the relaxation of the transverse magnetization is exponential (R_2 = 124 s^{-1}), but the relaxation of longitudinal magnetization is highly nonexponential due to spin-diffusion effects (initial decay rate constant of 28 s^{-1} and a slower rate of ~2.5 s^{-1} after equilibration of spin polarization). Neither a rigid-rod model nor simple wormlike motions can account for the observed low-temperature relaxation behavior. However, when localized internal motions of the base pairs (three-state jump model) are allowed for, a good fit of the experimental data is obtained by using a correlation time for internal motion of 7 × 10^{-10} s and an angular displacement of the bases of ±32° relative to the helix axis. The observed R_2/R_1 ratio for the thymine imino proton yields a value of 1.14 ± 0.08 Å for the imino proton nitrogen distance. Nuclear Overhauser effect (NOE) measurements establish that the base pairing in poly(dA-dT) is Watson–Crick in solution and not Hoogsteen. Exchange of the T-imino protons with H_2O dominates the longitudinal relaxation above 28 °C (activation energy of 17 ± 2 kcal and an exchange rate of 5 ± 2 s^{-1} at 300 K). Similar values have been reported for the A·T base pairs in DNA restriction fragments and for A·U base pairs in poly(A)·poly(U). These observations can be explained by a model in which exchange of T-imino protons occurs as a result of a single base pair opening, with a rate that is approximately independent of nearest-neighbor sequences and DNA length. Our observations appear to be inconsistent with a soliton model of proton exchange.

Recent discoveries in molecular biology (Reddy et al., 1978; Anderson et al., 1981; McKnight & Kingsbury, 1982; Moreau et al., 1982) and success in crystallographic studies on short DNA duplexes of defined sequence (Wang et al., 1979; Drew et al., 1981; Dickerson et al., 1982; Fratini et al., 1982) have focused new attention on various conformational and dynamic aspects of DNA structure. Poly(dA-dT) is one of the synthetic DNAs that has been the subject of a number of different studies (Brahms et al., 1976; Greve et al., 1977; Klug et al., 1979; Vorlickova et al., 1980; Marky et al., 1981; Viswamitra et al., 1982; Patel & Canuel, 1976, 1977; Patel, 1978; Shindo, 1981). Renewed interest in this molecule has been generated by recent CD studies that suggest that it adopts a bizarre structure in CsF (Vorlickova et al., 1980) and by recent proposals that the X-ray diffraction results can be interpreted in terms of a left-handed helix with Hoogsteen base pairing (Drew & Dickerson, 1982; Radwan & Wilson, 1982), although various other models have also been suggested (Arnott et al., 1974; Klug et al., 1979; Mahendrasingam et al., 1983). In the present studies, we have used a variety of NMR relaxation methods to examine the low-field NMR properties of short poly(dA-dT) duplexes.

From measurements of the spin–lattice (R_1) and spin–spin relaxation rates of the exchangeable thymine imino protons in A·T base pairs of poly(dA-dT), we obtain information about the N–H···N hydrogen bond length, base pair opening rates, and the effect of temperature on these rates. In addition, nuclear Overhauser effect measurements have been used to establish the base pairing structure (Figure 1). The spin–lattice relaxation measurements also provide evidence for pronounced spin-diffusion effects in poly(dA-dT). Since these effects were first noted in poly(dA-dT) (Kearns et al., 1981), we have found evidence for spin diffusion in many other DNAs. A general analysis of spin dynamics in DNA is developed and then specifically applied to poly(dA-dT) to estimate amplitudes and frequencies of local conformational fluctuations in the poly(dA-dT) base pairs.

Materials and Methods

The sodium salt of poly(dA·dT) was purchased from Miles Laboratories (lot no. 55A) and P-L Biochemicals (lot no. 658/92). The sample was sonicated for 6$^1/_2$ h in 1 M NaCl, pH 7, and prepared for NMR as described previously (Granot et al., 1982). The NMR samples contained approximately 48 mM in phosphates, 0.3 M NaCl, and 15 mM cacodylate, pH 7.01.

Sample size (53 ± 15 base pairs)[1] was evaluated by running ^{32}P-end-labeled aliquots on 8% polyacrylamide slab gels (nondenaturing conditions) along with markers from an *Hae*III digestion of pBR322, which covered a size range from 7 to 500 base pairs. The possibility that the NMR samples contained hairpins (Baldwin, 1971) was tested by taking two aliquots from the NMR tube, boiling and cooling one of them under suitable conditions to force hairpin formation, and sizing both samples as described above. The median size of the boiled aliquot was approximately half that of the untreated one, indicating that the original sample was not hairpinned.

Low-field (10–15 ppm) NMR spectra of poly(dA-dT) were measured on three different spectrometers: a Varian HR-300 spectrometer equipped with a Nicolet 1180 computer and operating at 300 MHz; a Nicolet-200 spectrometer equipped with a Nicolet 1180E computer and operating at 200 MHz; a 360-MHz spectrometer based on an Oxford Instrument

† From the Department of Chemistry, University of California—San Diego, La Jolla, California 92093. *Received July 19, 1983.* This work was supported by the American Cancer Society (Grant CH-32) and the National Science Foundation (Grant PCM-7911571).

* Address correspondence to this author at the Department of Chemistry, University of California—San Diego, La Jolla, CA 92093.

‡ Present address: Salk Institute, La Jolla, CA 92112.

§ Present address: Fonar Corp., Melville, NY 11747.

[1] All reported errors represent the standard deviation.

0006-2960/84/0423-0944$01.50/0

magnet and Nicolet 1180E computer. Selective excitation of the low-field imino resonances was achieved by applying long, medium strength radio frequency (rf) pulses (Early et al., 1980). With the modified time-shared Redfield-214 pulse sequence (Redfield & Kunz, 1979; Wright et al., 1981), and the rf carrier frequency set at the center of the imino resonances [between 13 and 14 ppm downfield from tetramethylsilane (Me_4Si)], the major effect of these pulses is on the low-field resonances, although a 180° pulse at 13 ppm noticeably excites resonances located in the region between 8 and 7 ppm (aromatic and amino protons). The effect of this excitation on the relaxation behavior of the low-field resonances will be discussed in a later section.

Nonselective excitation of all proton resonances was achieved by either of two methods. One method involved a 90°–τ–90° hard pulse sequence with a 100-ms homospoil during the delay time to destroy the transverse magnetization. The other method was a saturation–recovery experiment in which spins were saturated by application of a long, low-intensity rf pulse at the imino peak. The main effect of this pulse was to saturate the DNA proton resonances, although the water peak intensity decreased by ~5% after a 10-s irradiation of the imino proton (1 °C).

Longitudinal relaxation times ($T_1 = R_1^{-1}$) were measured by the inversion recovery method, and transverse relaxation times ($T_2 = R_2^{-1}$) were measured by the Hahn spin-echo method (sample nonspinning) (Hahn, 1950). Temperatures were varied by passing cooled or heated nitrogen or air through the probe and were stabilized to within ±1 °C.

The viscosity of the poly(dA·dT) NMR sample was determined by measuring the time required for 75 μL of the sample to partially drain from a drawn Pasteur pipet previously calibrated with H_2O and sucrose solutions of known viscosity. The relative viscosity (compared to H_2O) of the DNA solution was found to be 1.23 at 4 °C and 1.17 at 24 °C.

The base pairing structure of poly(dA-dT) was established by truncated NOE difference spectroscopy (TNOE) (Wagner & Wüthrich, 1979) in which difference spectra were recorded with the pulse sequence $[-P_1(\text{on-resonance})-P_{obsd}-t_1-P_1(\text{off-resonance})-P_{obsd}-t_1]_n$. The system was excited for various times P_1 by a selective low-power pulse alternately at or away from the imino resonance and allowed to relax for time t_1 after the observation pulse. In our studies a time-shared Redfield pulse sequence was used for P_{obsd}, the observation pulse.

Results

Watson–Crick Base Pairing in Poly(dA-dT). It is generally assumed that poly(dA-dT) exists in the Watson–Crick base pairing geometry. However, recent reports (Drew & Dickerson, 1982; Radwan & Wilson, 1982), based on reevaluation of fiber X-ray diffraction patterns, raise the possibility that the A·T base pairs may adopt the Hoogsteen base pairing geometry (Figure 1A) in which the imino proton is located close to the AH8 base proton (~2.8 Å). In the Watson–Crick base pair, the imino proton is located close to the AH2 proton (~2.85 Å) but distant from the AH8. Since the initial buildup rates of NOEs are inversely proportional to the sixth power of the distance between the observed and the presaturated proton (Noggle & Schirmer, 1971), TNOEs can be used to determine which proton (AH2 or AH8) is closer to the imino proton. Figure 1B clearly shows that magnetization from the imino proton is initially transferred to the AH2 proton with a chemical shift at 7.1 ppm (Patel, 1978). The AH8 resonance at 8.25 ppm is virtually unaffected until after much longer irradiation times. We thus conclude that poly(dA-dT) in a 0.1 M NaCl solution exists in the Watson–Crick base pairing conformation and not the Hoogsteen geometry.

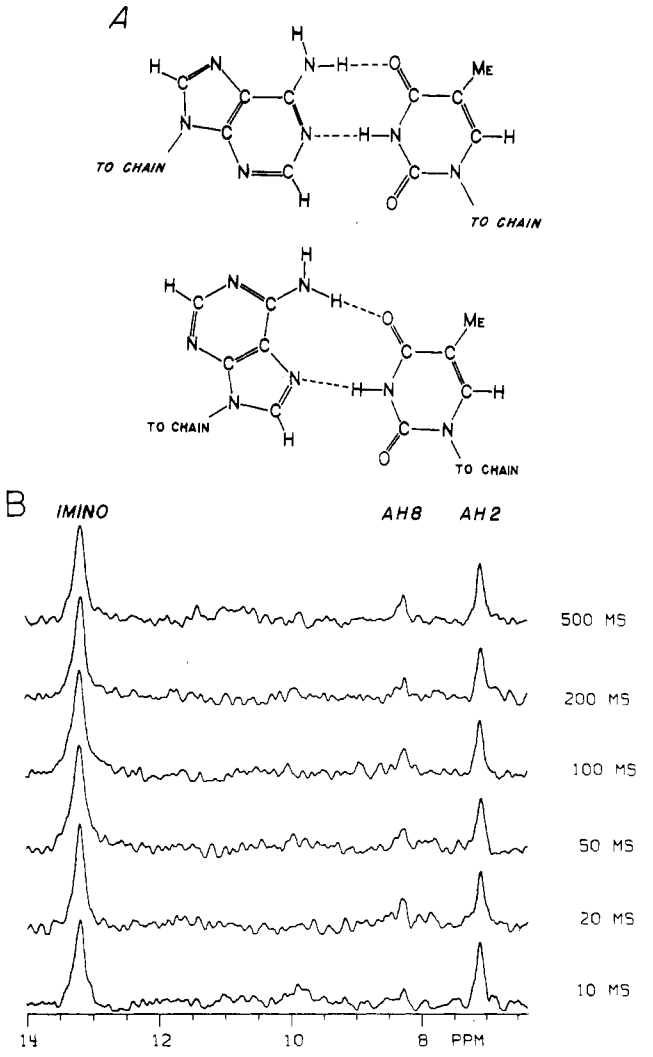

FIGURE 1: (A) Proposed base pair structures for poly(dA-dT): Watson–Crick and Hoogsteen geometry. (B) TNOE difference spectra resulting from irradiation at imino resonance for the times indicated at the right of the figure. The spectra shown demonstrate strong transfer of magnetization from imino proton (13.17 ppm) to AH2 (7.07 ppm) and much weaker transfer to AH8 (8.24 ppm).

Temperature Dependence of Relaxation Rates: Distinction between the Dipolar and Exchange Contributions to Relaxation. Spin–lattice (R_1) and spin–spin (R_2) relaxation rates of the low-field resonances in poly(dA-dT) were measured in the temperature range 1–38 °C at 300 MHz, and typical relaxation spectra (20 °C) are presented in Figure 2. The spin–spin relaxation was exponential at all temperatures, and the rates, R_2, ranged from 124 s^{-1} at 1 °C to 59 s^{-1} at 38 °C. The observation of single exponential decay of the transverse magnetization indicates that the sample is relatively homogeneous (see Appendix B).

Spin–lattice relaxation curves at three different temperatures (1, 21, and 38 °C) are shown in Figure 3. At low temperatures, where magnetic dipolar contributions to relaxation dominate, the relaxation curves are highly nonexponential because of spin diffusion (see below). However, as the temperature is increased, exchange becomes more important until at high temperatures exchange dominates the spin–lattice relaxation and the recovery curves are exponential.

The nonexponential recovery of the longitudinal magnetization can be approximately characterized by two limiting rates: the initial slope of the decay curve, R_1 (initial), and a slower rate obtained as the limiting slope at longer times,

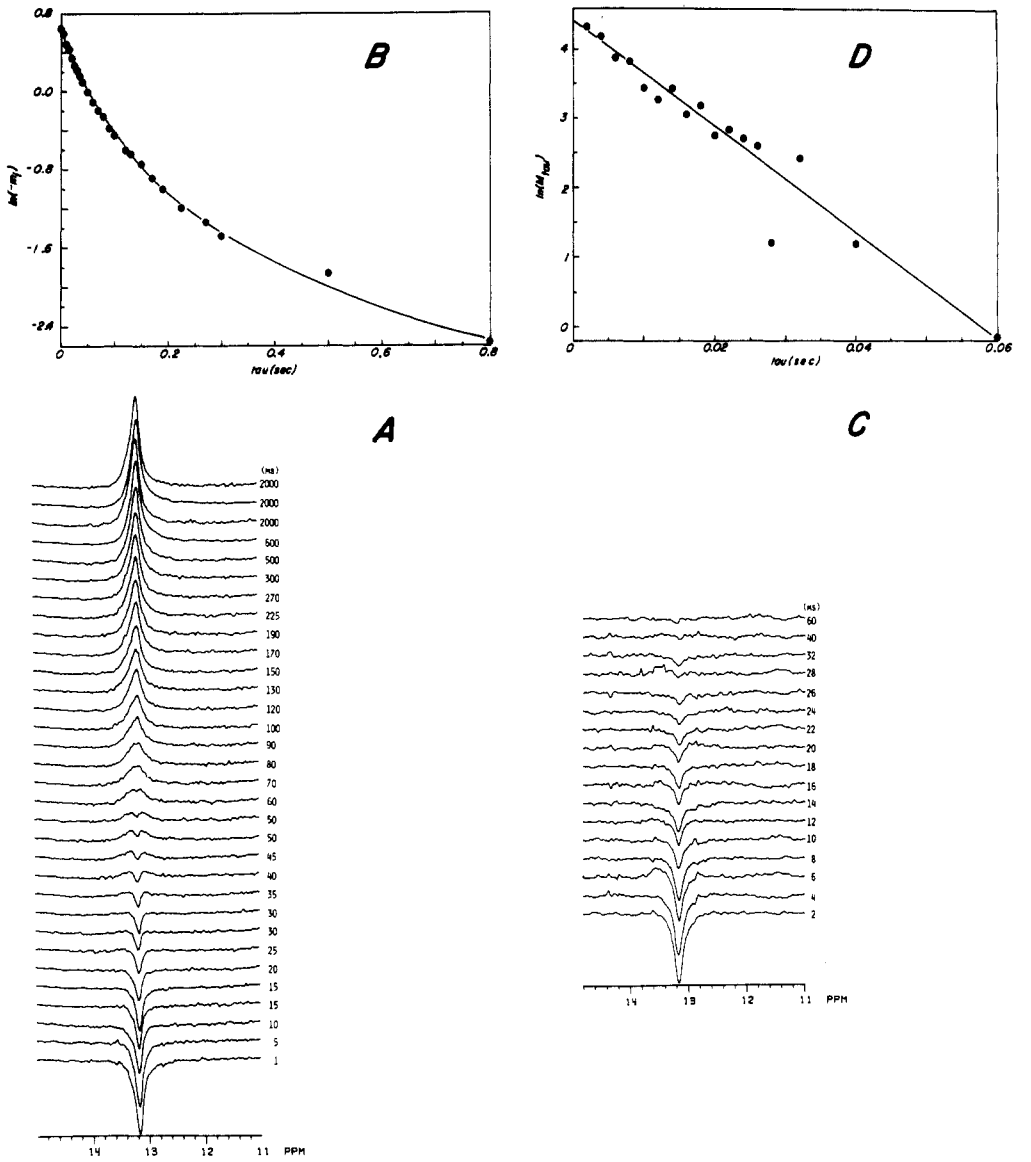

FIGURE 2: ^{1}H spectra (A, C) and semilog plots (B, D) showing relaxation of imino proton in poly(dA-dT). (A and B) Recovery of longitudinal magnetization; (C and D) recovery of transverse magnetization at 300 MHz and 20 °C.

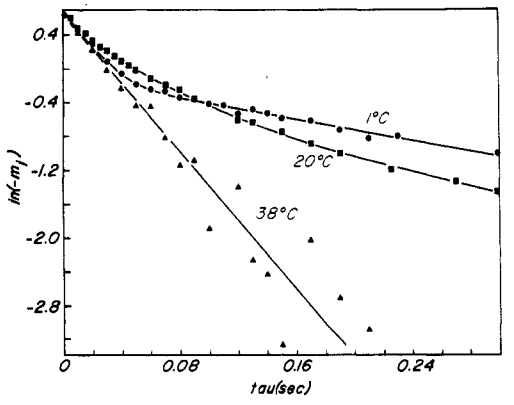

FIGURE 3: Effect of temperature on the relaxation of the longitudinal magnetization in poly(dA-dT). The temperatures were 1 (●), 20 (■), and 38 °C (▲).

R_1(long). The temperature dependence of R_2 and of the initial fast and slow components of the longitudinal magnetization is summarized in Figure 4. The reduction in R_2 and R_1 (initial) as the temperature increases from 0 to 18 °C results from more rapid tumbling of the DNA molecule at higher temperatures due to decreased solvent viscosity. The increase in R_1(initial) and R_2(long) above 20 °C is attributed to proton exchange with the solvent. The exchange results from random "opening" of the A·T base pairs and permits thymine imino protons to exchange with the bulk water protons with a rate that increases with temperature until the double helix melts (Teitelbaum & Englander, 1975a,b). To evaluate exchange and dipolar contributions to the relaxation rates, relaxation data were analyzed by using the relation

$$R_i^{obsd} = R_i^d + R_{ex} \quad (1)$$

where R_i^{obsd} denotes the experimentally measured values of either the transverse ($i = 2$) or the longitudinal ($i = 1$) relaxation rates, R_i^d denotes the dipolar contribution to the relaxation, which decreases with temperature, and R_{ex} is the rate of exchange of the imino protons. The temperature dependence of the two mechanisms contributing to the relaxation may be written as (Abragam, 1961)

$$R_i^d = R_i^o \exp[E_a^i/(RT)] \quad (2)$$

and (Teitelbaum & Englander, 1975a)

$$R_{ex} = R_{ex}^0 \exp[-E_a^{ex}/(RT)] \quad (3)$$

where E_a^i and E_a^{ex} denote activation energies. The relaxation data were analyzed with eq 1–3 by a least-squares fitting program, and the best-fit parameters are given in Table I. The

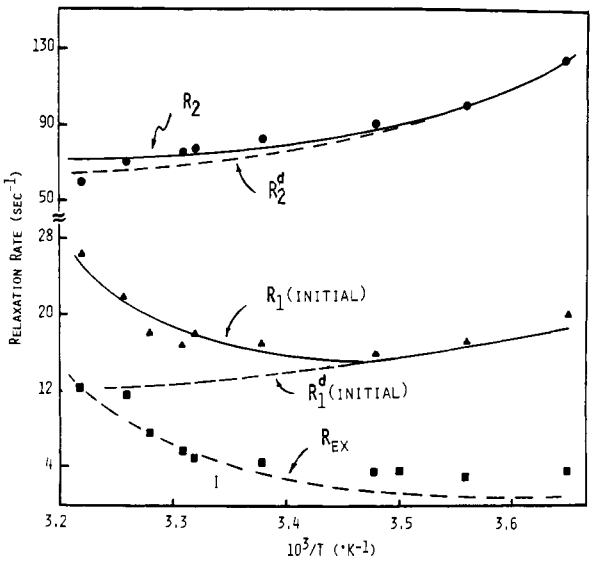

FIGURE 4: Temperature dependence of relaxation rates for imino proton in poly(dA-dT). The R_2 (●), R_1(initial) (▲), and R_1(long) (■) values used in exchange calculations are plotted vs. $1/T$. The values for R_1(initial) and R_1(long) were taken from the slopes of the relaxation curve at short times and long times, respectively. The dashed line R_{ex} represents the calculated exchange contribution to the imino proton relaxation. R_1^d(initial) and R_2^d represent the calculated dipolar contribution to exchange to the observed relaxation rates. The solid curves through the points are the sum of the exchange and dipolar contributions.

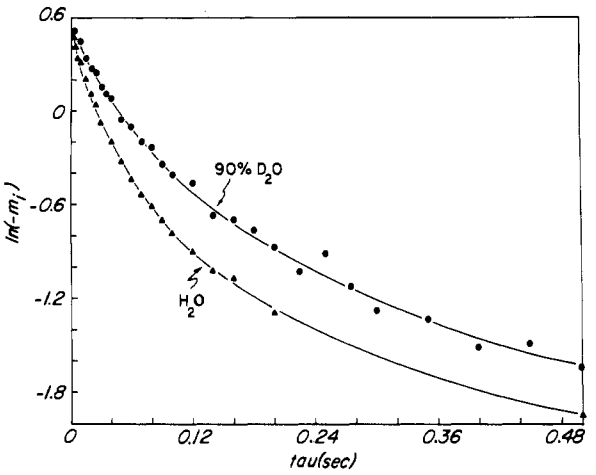

FIGURE 5: Recovery of longitudinal magnetization at 360 MHz and 1 °C for imino proton when solvent is 100% H_2O (▲) or 10% H_2O/90% D_2O (●).

Table I: Calculated Activation Energies and Preexponential Factors for Relaxation and Exchange Rates in Poly(dA-dT) at 300 MHz

process	$R^{0\,a}$ (s^{-1})	$E_a{}^a$ (kcal/mol)
transverse relaxation (dipolar)	0.27 ± 0.05	−3.4 ± 0.6
longitudinal relaxation (init) (dipolar)	0.28 ± 0.05	−2.3 ± 0.4
longitudinal relaxation (slow) (dipolar)	*b*	*b*
exchange rate	(9.0 ± 0.5) × 10^{12}	17 ± 2

[a] $R = R^0 \exp[-E_a/(RT)]$. [b] Data did not allow accurate determination of these parameters.

exchange contribution to the relaxation rates is estimated to vary from 0.25 s^{-1} at 1 °C to 12 s^{-1} at 38 °C.

Effect of Deuteration on Relaxation. Figure 5 depicts the effect of 90% deuteration on the imino proton relaxation at

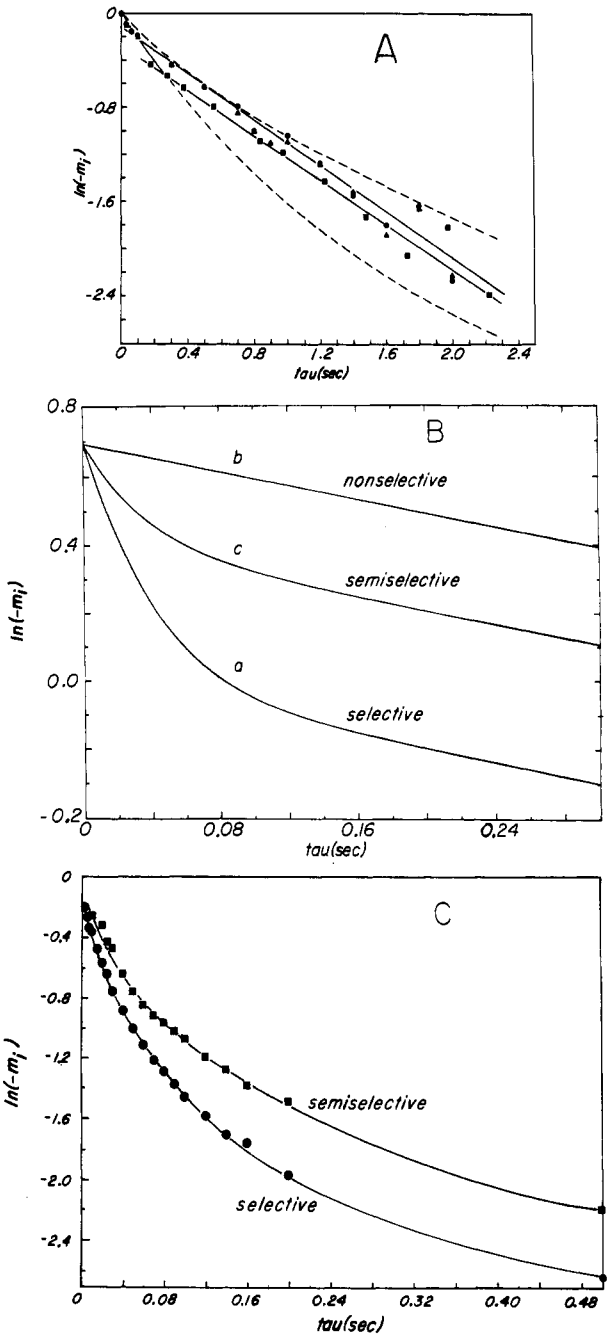

FIGURE 6: (A) Semilog recovery curves for nonselective relaxation of imino proton in three different experiments: observed curves after (■) 90° hard pulse or after (●) 1-s or (▲) 4-s saturation of the imino proton resonance. Relaxation curves calculated for limiting sets of relaxation parameters (---) (see Appendix A). (B) Calculated longitudinal magnetization relaxation curves in a model two-spin system for different preparation pulses: (a) selective inversion of nucleus i, (b) nonselective inversion of both nucleus i and nucleus s, and (c) semiselective inversion of nucleus i (nucleus i received π pulse and nucleus s received $\pi/2$ pulse). (C) Comparison of imino proton longitudinal relaxation in poly(dA-dT) at 360 MHz and 1 °C after selective excitation (●) and semiselective excitation (■) using time-shared Redfield sequence.

1 °C. At this temperature, the relaxation is due to magnetic dipolar interactions since the estimated exchange contribution to the relaxation of the imino protons is small ($R_{ex} < 0.25$ s^{-1}). The 50% deuteration (data not shown) has little effect on the longitudinal relaxation, but 90% deuteration decreases the initial relaxation rate by ~50% compared to that in water.

Nonselective Longitudinal Relaxation of the Imino Proton in H_2O. The recovery of the longitudinal magnetization of the imino protons following nonselective excitation of all

protons in the DNA in H_2O at 1 °C is shown in Figure 6. The recovery of the magnetization is single exponential with a rate of 1.0 ± 0.1 s^{-1}.

Magnetic Dipolar Contribution to Spin–Lattice Relaxation. (A) General Theoretical Considerations. The relaxation of the longitudinal magnetization of a nucleus i (e.g., the imino proton) due to magnetic dipolar interactions with other nuclei, s, can be described by differential equations of the form (Noggle & Schirmer, 1971; Kalk & Berendsen, 1976)

$$dm_i/dt = -\sum_{s\neq i}\rho_{is}m_i - \sum_{s\neq i}\sigma_{is}m_s \quad (4)$$

where $m_i = (M^i_{zt} - M^i_{zo})/M^i_{zo}$, M^i_{zt} is the longitudinal magnetization of nucleus i at time t, and M^i_{zo} is the the equilibrium longitudinal magnetization, and similarly for m_s. The quantities ρ_{is} and σ_{is} are defined as

$$\rho_{is} = K[J_0(\omega_i - \omega_s) + 3J_1(\omega_i) + 6J_2(\omega_i + \omega_s)] \quad (5)$$

$$\sigma_{is} = K[-J_0(\omega_i - \omega_s) + 6J_2(\omega_i + \omega_s)] \quad (6)$$

$$K = 2\gamma_i^2\gamma_s^2\hbar^2S(S + 1)/(3r_{is}^6) \quad (7)$$

I and S are the spins of nuclei i and s, r_{is} is the internuclear distance between nucleus i and nucleus s, γ_i and γ_s are the gyromagnetic ratios, ω_i and ω_s are the Larmor frequencies for nuclei i and s, and $J_n(\omega)$ (n = 0, 1, 2) values represent the spectral densities. The $J_n(\omega)$ values depend on the motional properties of the system, and for large, slowly tumbling molecules like DNA, $J_0 \gg J_1, J_2$. The ρ_{is} term represents the transfer of magnetization away from spin i; the J_0 term represents adiabatic transfer of magnetization from nucleus i to nucleus s, and the J_1 and J_2 terms represent one- and two-quantum transitions that transfer magnetization directly to the lattice. The cross-relaxation term, σ_{is}, expresses the transfer of magnetization from nucleus s back to nucleus i via zero-quantum transitions and transfer to the lattice by two-quantum transitions. To emphasize the fact that the recovery of m_i depends on the magnetization of both the i and the s spins, eq 4 can be rewritten for two spins as

$$dm_i/dt = -Km_i[J_0(\omega_i - \omega_s) \times (1 - m_s/m_i) + 3J_1(\omega_i) + 6J_2(\omega_i + \omega_s)(1 + m_s/m_i)] \quad (8)$$

where the contribution of the J_0 and J_2 spectral densities to the spin–lattice relaxation of nucleus i depends on the ratio of magnetization present in nucleus i and nucleus s. This differential equation allows us to consider the relaxation kinetics for the different types of experiments that can be performed.

Figure 6B illustrates the relaxation of spin i in a two-spin system where R_1(sel) = 16 s^{-1} and R_1(long) = 1 s^{-1} after selective excitation of just the imino proton and semiselective (excitation of imino protons with partial excitation of other protons) or nonselective excitation of all protons. It is obvious from these curves that the relaxation rate observed when $m_i = m_s$ is equal to the nonselective rate, R_1(long), independent of the initial state of the system. In addition, when the slope of the relaxation curve from 0 to 20 ms was measured after selective excitation, it was found that this method gives an R_1(initial) that is less than 86% of R_1(sel). This indicates that for any system where R_1(sel) is significantly larger than the nonselective rate, the true selective rate constants cannot simply be measured from the slope of the relaxation curve. Instead, a kinetic analysis of the entire relaxation curve must be performed to extract the rate constants.

The kinetic analysis of relaxation in a two-spin system can easily be extended to more than two spins. The *rate constant* describing the initial relaxation is R_1(sel) = $\sum_{s\neq i}\rho_{is}$. If the spins of interest are strongly coupled to one another and are relatively isolated from other spins, the rapid zero-quantum transfer of magnetization will tend to equalize the magnetizations of all the spins in the group (referred to as an "island" of spins). After the magnetizations of all spins in the island are equalized, they will relax collectively via transfer of magnetization to the lattice or to other spin islands located nearby. Although the rate of magnetization transfer away from the island may be different for each spin, the observed relaxation rate of any spin will be the average relaxation rate of all the spins because they are strongly coupled by zero-quantum transitions.

Table II: Representative Interproton Distances Obtained from X-ray Coordinates

atom pair	model 1[a] distance (A)	model 2[b] distance (A)
TH3–TN3	1.14[c]	1.14[c]
TH3–AH61	2.46	2.35
TH3–AH2	2.85	3.29
TH3–TH3 above	4.01	4.84
TH3–TH3 below	4.12	4.61
AH61–AH62	1.75	1.72
AH61–AN6	1.01	1.01
AH62–AN6	1.01	1.01

[a] Protons were added to atomic coordinates from Arnott et al. (1983). [b] Protons were added to atomic coordinates from Klug et al. (1979). [c] This distance is a fitted parameter in the calculations.

Table III: Comparison of Measured and Calculated Rate Constants for Imino Proton Relaxation at 1 °C after Selective and Semiselective Excitations

	R_1(sel) (s^{-1})		R_1(long) (s^{-1})	
excitation	initial slope[a]	kinetics[b]	slope[c]	kinetics
selective	23 ± 3	28 ± 3	2.4 ± 0.2	2.3 ± 0.01
semiselective	17 ± 1	27 ± 3	2.5 ± 0.2	2.56 ± 0.01

[a] Straight line fit of initial slope of decay curve. [b] Fit of the complete decay curve. [c] Straight fit of decay curve at long times.

(B) Analysis of the Imino Proton Spin–Lattice Relaxation in Poly(dA-dT) at 1 °C. This relaxation curve, following a selective excitation of the imino resonance at 13.2 ppm (Figure 6C), was analyzed with a kinetics scheme where the rate constants ρ_{is} were assumed proportional to r_{is}^{-6}. The interatomic distances were taken from four different X-ray structures (Arnott et al., 1974, 1983; Klug et al., 1979) with protons added to the atomic coordinates. Distances for two of these structures are shown in Table II. Each ρ_{is} (and σ_{is}) for the kinetics calculation was first calculated assuming that there was no internal motion. In all cases, this gave initial relaxation rates that were much too large. The values of ρ_{is} were then scaled by some factor until the calculated curve matched the observed relaxation curve. The value for the scaling constant differed for each model, but the value calculated for R_1(sel) was insensitive to the model used in fitting the curve. The rate obtained by measuring the slope of the initial relaxation of the experimental curves and rate constants obtained from the kinetics fit are compared in Table III. Note that the value of R_1(sel) determined by analysis of the decay curve (28 s^{-1}) is 22% larger than the rate of 23 s^{-1} determined from straight-line extrapolation of the early time selective relaxation behavior.

Several semiselective experiments were analyzed in the same manner, and the rate constants obtained agree with the results obtained from analysis of the selective relaxation experiment

(Table III). This analysis also indicated that the Redfield pulse inverted the imino proton ~84° and the AH2 and amino protons ~25° in agreement with the degree of excitation expected from the Fourier analysis of the exciting pulse (R. W. Behling, unpublished results). Excitation of the AH2 and amino protons is the reason that the initial relaxation rate determined from the initial slope of the decay curve after the semiselective excitation is slower than that after the selective excitation and also explains why the relaxation curve bends sooner than it does after selective excitation. Analysis of all the 1 °C imino relaxation data at 360 MHz yields the following average values: R_1(sel) (calculated) = 28 ± 4 s^{-1} and R_1(long) (calculated) = 2.4 ± 0.2 s^{-1}.

Although we were able to account for the relaxation of the imino proton in both the selective and semiselective relaxation experiments using a model containing only four interacting spins (i.e., the imino, AH2, and the two amino protons pictured in Figure 1A),[2] nonselective excitations of the DNA were performed (results shown in Figure 6A) to test whether all pertinent interactions had been included. In these experiments, *all* of the nuclei in the DNA (exchangeable and nonexchangeable protons) were given a magnetization $m_i = -1$, and the recovery of the imino proton magnetization was measured. If the four-spin island were truly isolated from all other nuclei in the DNA, then nonselective excitation of all the nuclei in the DNA molecule should result in the same R_1(long) already determined for the imino proton by observation of the long-time relaxation behavior in the experiments involving selective and semiselective excitation of the imino protons. However, if there are significant interactions between the four-spin island and other nuclei in the DNA, then a different rate could be observed. The observed nonselective relaxation rates, which range from 0.90 ± 0.03 to 1.03 ± 0.04 s^{-1}, are to be compared to the value of R_1(long) = 2.4 ± 0.2 s^{-1} obtained in the selective and semiselective excitation experiments. This difference in the long-time relaxation behavior following different initial states implies that there is an additional source of relaxation for the four-spin system not included in our initial analysis.

A detailed analysis of the relaxation behavior given in Appendix A indicates that the imino proton relaxation at long times after selective or semiselective excitation must include a component of magnetization transfer from the four-spin island[2] to surrounding protons (R_1), presumably the 19 nonexchangeable protons of the sugars and bases. The contribution to relaxation from these 19 other nonexchangeable protons would have been much smaller than between the protons within the island because these nuclei are relatively far away from the four protons in the island, but this is partially compensated for by the fact that these nonexchangeable protons are not excited by the initial pulse; thus, their contribution to the relaxation of the four-spin island occurs by zero-quantum processes. The analysis of the 1 °C spin–lattice relaxation of poly(dA-dT) (Appendix A) yields the following rate constants: R_1(sel) = 28 ± 4 s^{-1}, R_1(long) = 1.7 ± 0.3 s^{-1}, and R_1(4-spin to 19-spin) = 0.7 ± 0.3 s^{-1}. This analysis shows that the 2.4 s^{-1} rate observed for R_1(long) in the selective and semiselective experiments actually has two contributions. One of these is a 0.7-s^{-1} transfer of magnetization to the 19 nonexchangeable protons, and the other, 1.7 s^{-1}, is the relaxation rate to the lattice that would be observed if the four-spin island were truly isolated from all other spins. The significance of these rate constants in terms of the structure and dynamics of poly(dA-dT) is considered under Discussion.

Table IV: Comparison of Experimental Rates at 1 °C with Rates Calculated Using Rigid-Rod Model[a]

	calculated (s^{-1})	experimental (s^{-1})
R_1(sel)	85.4	28 ± 4
R_1(long)	0.04	1.7 ± 0.3
R_2	371	124 ± 12

[a] $\tau_l = 5.1 \times 10^{-7}$ s; $\tau_s = 3.6 \times 10^{-8}$ s.

Magnetic Dipolar Contribution to Spin–Spin Relaxation. The transverse relaxation rate due to dipolar interactions between unlike spins i and s is given by (Abragam, 1961)[3]

$$R_2 = [\gamma_i^2\gamma_s^2\hbar^2S(S+1)/(3r^6)] \times [4J_0(0) + J_0(\omega_i - \omega_s) + 3J_1(\omega_i) + 6J_1(\omega_s) + 6J_2(2\omega_i)] \quad (9)$$

where the variables are the same as those defined for eq 5–7. A similar equation applies to the interaction between like spins.

Note that unlike the spin–lattice relaxation rate, the transverse relaxation rate is unaffected by spin diffusion, and therefore, relaxation will be exponential, provided that scalar interactions are absent. The above theoretical expression must be used to account for the observed R_2 = 124 ± 12 s^{-1} at 1 °C.

Analysis of Relaxation Rates Using Models for Internal Motion in Poly(dA-dT). Relaxation rates provide important information about the structure and dynamics of a molecule. Although the motions of the atoms in a macromolecule like DNA may be quite complex, simplified motional models may be used to obtain estimates of amplitudes and correlation times of the actual motions present. Since these models can only approximate the true molecular motions, the data should be fit by using the simplest model possible. More complex models should be invoked only if calculations made with the simple models do not fit the data.

The DNA used in the present study (53 base pair) is much shorter than the persistence length of DNA (~200 base pair) and, therefore, behaves hydrodynamically as a rigid rod in solution (Hagerman, 1981; Charney & Yamaoka, 1982) with overall motions described in terms of two correlation times: τ_l for motion about the short axis of the DNA (end-over-end tumbling) and τ_s for motion about the long axis of the DNA (axial spinning). The spectral densities arising from the diffusional motion of a rigid rod are given by (Woessner, 1962)

$$J_n(\omega) = \frac{1}{5}\sum_{i=1}^{3} A_i \frac{\tau_i}{1 + \omega^2\tau_i^2} \qquad n = 0, 1, 2 \quad (10)$$

where $A_1 = {}^1/_4(1 - 3\cos^2\theta)^2$, $A_2 = 3\sin^2\theta\cos^2\theta$, $A_3 = {}^3/_4\sin^4\theta$, $\tau_1^{-1} = \tau_l^{-1}$, $\tau_2^{-1} = {}^5/_6\tau_l^{-1} + {}^1/_6\tau_s^{-1}$, $\tau_3^{-1} = {}^1/_3\tau_l^{-1} + {}^2/_3\tau_s^{-1}$, and θ is the angle between the internuclear (I–S) vector and the long axis of the DNA molecule.

The rotational correlation times for a rigid rod of length L and radius b in a solution with viscosity η can be approximated by using the semiempirical relations of Broersma (1960). The viscosity of the poly(dA-dT) sample relative to water at 1 °C is 1.24, implying that the solution viscosity is η = 0.021 P. At this viscosity, a 53 base pair piece of DNA behaving as a rod of length L = 180 Å and radius b = 13 Å will have $\tau_l = 5.1 \times 10^{-7}$ s and $\tau_s = 3.6 \times 10^{-8}$ s.

Relaxation rates were calculated by using these values of τ_l and τ_s and interproton distances and angles which were

[2] We shall refer to this collection of spins as a four-spin island.

[3] For unlike spins $\Delta\nu = (\nu_i - \nu) > R_2/\pi$.

Table V: Parameters Used in Three-State Jump Model To Fit Experimental Relaxation Data at 1 °C, 360 MHz

parameter	range searched	minimum fit[a]	maximum fit[a]	average[b]
τ_{int} (s)	10^{-11}–10^{-7}	10^{-10}	10^{-9}	$(4.4 \pm 3.4) \times 10^{-10}$
amplitude of internal motion (deg)	0–±50	±30	±36	±32 ± 2
r_{NH} (Å)	1.00–1.50	1.00	1.3	1.14 ± 0.08
R_1(sel) (s^{-1})	28 ± 20%			28 ± 2
R_1(long) (s^{-1})	1.7 ± 20%			1.70 ± 0.34
R_3 (s^{-1})	124 ± 10%			123 ± 7

[a] For the various combinations of the parameters that produce fits of the data, these values represent the extremes observed for each variable. [b] Average and standard deviation calculated by using parameter values that produce fits of the relaxation rates.

obtained from various X-ray structures for poly(dA-dT) to which protons had been added to the heavy atom coordinates. The important interproton interactions for two of the structures are presented in Table II, and a comparison of rates calculated by using the rigid-rod model and experimental rates is presented in Table IV for Klug's B-form structure (Klug et al., 1979), with similar results obtained for the other structures considered. Inspection of Table IV shows that there are major disagreements between the experimental rates and the rates calculated when the rigid-rod model is used; specifically, we find that calculated values of R_1(sel) and R_2 are much larger (factor of 3) than the experimental values, while the calculated value of R_1(long) is ~40 times too small. Both disagreements can be corrected by allowing for internal motions of the base pairs in the DNA since these will decrease J_0 [the major contribution to R_1(sel) and R_2] while increasing both J_1 and J_2 [major contribution to R_1(long)].

Lipari & Szabo (1982) have demonstrated that a variety of different models for internal motion can be used to interpret relaxation data, often with comparable success. Fortunately, different models typically yield similar correlation times and comparable amplitudes for the motions, although the nature of the motions may in fact be quite different. Recognizing this limitation, we used a three-state jump model (Woessner et al., 1969) to include effects of internal motions (similar results were obtained when a wobbling cone model or two-state jump model was used). The spectral densities are similar in form to those in eq 10 but contain terms that depend on the angle between the internuclear vector and the helix axis, the angle between the internuclear vector and the axis about which internuclear internal motion occurs, and the internal motion correlation time which describes the reorientation of the internuclear vector between the different jump sites.

Many parameters can be varied in calculating the relaxation rates, and given our limited amount of NMR data, we were unable to constrain the structure sufficiently to produce a unique result. We therefore used interproton distances from four different sets of X-ray coordinates to determine if any of them could be eliminated as a possible structure for poly(dA-dT) in solution. Having fixed the interproton distances and the angles between the internuclear vectors and the helix axis by using values from the X-ray structures, we varied the internal motion correlation time, the amplitude of internal motion, and the bond length between the imino proton and the imino nitrogen, TN3. We find for a given viscosity (which determines τ_1 and τ_s) the amplitude of internal motion is largely determined by how much the J_0 term must be decreased in order to fit R_1(sel). Within this angular fluctuation, R_1(long) must then be fit by adjusting τ_{int}. In addition, once the amplitude of internal motion is constrained to fit R_1(sel), the proton contribution to R_2 is also fixed. R_2 is then uniquely sensitive to small changes in the distance between the imino proton and TN3 (r_{NH}) (via the J_0 term in eq 9) since ~40% of the transverse relaxation is due to the N–H dipolar interaction, according to our analysis.

The actual calculations were carried out by incrementing each parameter over a range while all other parameters were held fixed, thereby calculating the rates for each incremental value in the three-dimensional space defined by the variable parameters mentioned above. Those combinations that simultaneously fit the observed rates within experimental error (±20% for R_1(sel) and R_1(long) and ±10% for R_2) were recorded. The ranges of values searched for each parameter, along with ranges of each parameter that fit the calculated data, are given in Table V.

This analysis shows that, independent of the specific structure used, three features were common to all of the structures: (1) the amplitude of internal motion (relative to the helix axis) required to fit the experimental relaxation rates is between 30° and 36° and averages ±32° (±2°), (2) r_{NH} for the imino proton must be about 1.14 ± 0.08 Å, and (3) τ_{int} ranges from 1×10^{-10} to 2.5×10^{-9} s and averages about 7×10^{-10} s.

Effect of Deuteration on Relaxation. The relaxation curves obtained in 50% and 90% D_2O/H_2O for poly(dA-dT) were simulated by using three base pair fragments $(ApTpAp)_2$ built from Arnott's D-form (Arnott et al., 1974) and Klug's B-form X-ray coordinates (Klug et al., 1979). Imino proton relaxation curves calculated for the center A·T base pair in these models were compared to the experimental data (Figure 5). The calculated curves are virtually indistinguishable from one another at 50% deuteration, but Arnott's structure gives slightly better results at 90% deuteration. In these calculations using the three base pair fragments, the relaxation curves are too slow and bend too soon because relaxation of protons in the outer two bases has not been properly considered. This limitation, together with the similarity of the calculated curves, prevents us from distinguishing between these two X-ray structures based on the relaxation of the imino proton. However, analysis of the relaxation rates of aromatic protons allows us to distinguish between certain features of these and other models (Kearns, 1983; Kearns et al., 1983).

Field Effect on Spin–Lattice Relaxation Rates. The effect of magnetic field on relaxation was determined by comparing the relaxation of low-field resonances at 1 °C measured at 200, 300, and 360 MHz (Figure 7). In each instance, the relaxation was nonexponential, and the fast initial rate was found to be virtually the same at all three spectrometer frequencies. This is consistent with the dominance of the $J_0(0)$ term in eq 8 that renders the dipolar contribution to R_1(sel) field independent. R_1(long) (after subtracting the relaxation rate to the nonexchangeable protons) was found to be 2.5 s^{-1} at 200 MHz, 1.9 s^{-1} at 300 MHz, and 1.7 s^{-1} at 360 MHz. The fact that the rates are only slightly faster at lower frequencies is consistent with the presence of fast internal motions that significantly affect this relaxation rate. In the absence of internal motions, R_1(long) is expected to be 3.2-fold larger at 200 MHz than at 360 MHz. Analysis of the slowly relaxing component at 300 MHz, as described above, yields a range of correlation times similar to that obtained from the analysis

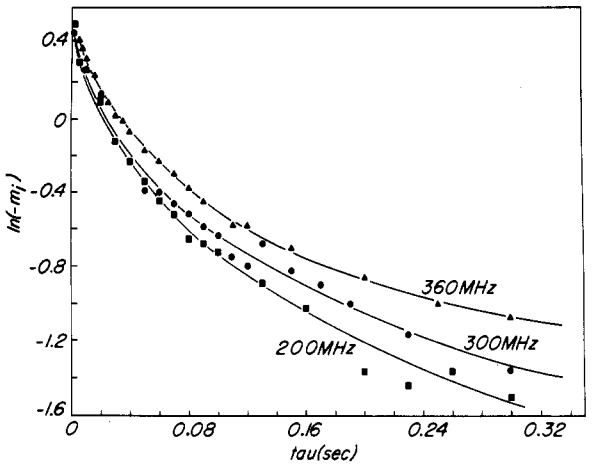

FIGURE 7: Comparisons of the semiselective spin–lattice relaxation of the imino proton of poly(dA-dT) at 1 °C at 360 (▲), 300 (●), and 200 (■) MHz.

of the 360-MHz data (τ_{int} between 0.1 and 1.0 ns) and similar amplitudes of motion (±31 ± 1°). The analysis of the 200-MHz data also gave similar amplitudes of motion, but τ_{int} ranged from 0.16 to 2.5 ns. Results from the three different magnetic fields indicate that the amplitude of internal motion averages ±32 ± 2° and τ_{int} ranges from 0.1 to 2.5 ns, with an average of 0.7 ns.

Discussion

Measurements of the imino spin–lattice and spin–spin relaxation rates presented here provide insight into structural and dynamic properties of one of the most well-studied synthetic DNAs, poly(dA-dT).

Analysis of the Low-Temperature Relaxation Rates. In the low-temperature regime, where relaxation rates are determined almost exclusively by magnetic dipolar interactions, the relaxation of the transverse magnetization is exponential (R_2 = 124 ± 10 s^{-1} at 1 °C), whereas the decay of the longitudinal magnetization is nonexponential (Figures 3 and 4). Exponential decay of the transverse magnetization indicates that poly(dA-dT) used in these experiments is relatively homogeneous (average size of about 53 base pairs). Therefore, the highly nonexponential behavior observed in measurements of the relaxation of the longitudinal magnetization could not have resulted from heterogeneity in the sample (e.g., due to a mixture of length and hairpins). Furthermore, the electrophoresis experiments comparing samples before and after boiling rule out the presence of hairpins. The effect of a size distribution on the observed R_1 and R_2 is discussed under Appendix B. We therefore attribute the nonexponential decay of the longitudinal magnetization to spin-diffusion effects.

Qualitatively, the spin–lattice relaxation behavior is as follows. Initial rapid decay of the magnetization arises from transfer of spin polarization from imino protons by zero-quantum processes to neighboring AH2 and amino protons until the magnetization is equalized among these four protons. Subsequently, zero-quantum transitions within this four-spin island effectively maintain equal spin populations, and the four interacting protons relax together to the lattice via one- and two-quantum processes which depend upon $J_1(\omega_H)$ and $J_2(2\omega_H)$. The four-spin island also continues to relax via zero-quantum processes with 19 nonexchangeable protons located relatively far away.

Computer analysis of the 1 °C decay kinetics of this four-spin system yielded a value of 28 ± 4 s^{-1} for the pure dipole–dipole contribution to the initial longitudinal relaxation rate, 1.7 ± 0.3 s^{-1} for a nonselective longitudinal relaxation rate at long times, and 124 ± 10 s^{-1} for a spin–spin relaxation rate.

That nonexchangeable protons contribute to the relaxation of the four-spin island is evidenced when all of the DNA proton resonances are excited by nonselective pulses (Figure 6). In these experiments, the relaxation is exponential with a rate, 1.0 ± 0.1 s^{-1}, which is more than a factor of 2 slower than the slow relaxation following selective or semiselective excitation of the imino proton. This 2-fold difference in rates indicates that the nonexchangeable protons have significant interactions with the protons in the four-spin island.

We initially used a rigid-rod model to describe the rotational diffusion of the DNA molecules and obtained the results shown in Table IV. With this model, the values for R_2 and R_1(sel) are found to be approximately 3 times larger than the experimental values, whereas the predicted value of R_1(long) is ~40 times too small. This clearly demonstrates that a rigid-rod model does not properly predict the relaxation behavior in poly(dA-dT). We therefore used a model which allowed for internal motions of the base pairs and for calculation purposes used a three-state jump model previously described by Woessner et al. (1969). With this model, we successfully fit the experimental data using a range of parameters, some of which are displayed in Table V. In particular, good fits of the experimental data were obtained assuming that the normal to the base planes make angular fluctuations of ±32° relative to the helix axis with a correlation time for internal motion on the order of 0.1–1.0 ns. Slightly different parameters for τ_{int} and θ would be obtained if a different model was used to incorporate the effects of internal motion, but we were unable to fit the observed relaxation data using angular fluctuations smaller than ±30° and internal motion correlation times outside the 0.1–2.5-ns range. We further conclude that there are no larger amplitude (> ±36°) motions with time constants between 1 and 500 ns since these would have further decreased the values of R_2 and R_1(initial) below those observed experimentally. Thus, we are led to a picture of poly(dA-dT) in which there are hindered ±32° motions of the bases relative to the helix axis with time constants between 0.1 and 1 ns but no larger amplitude internal motions up to 500 ns. Although slower bending motions of the DNA are undoubtedly present with the 53 base pair DNA, we are unable to detect longer time (internal) motions since they would exceed the molecular tumbling time.

In addition to obtaining information about the properties of poly(dA-dT), the above analysis provides a framework for analyzing the relaxation behavior in other simple sequence DNAs and more complicated DNAs. It will be interesting to see whether there are significant sequence effects on internal motions of DNA and the extent to which conformation (A, B, Z, and others) may affect the motion. Preliminary experimental results suggest that the high-frequency motions of bases in poly(dA-dT) and poly(dG-dC) (Mirau & Kearns, 1983) are rather similar.

It is interesting to compare the poly(dA-dT) results with those from other DNA samples. In previous studies, we measured low-temperature spin–lattice and spin–spin relaxation rates in random sequence DNA (Early et al., 1980a) and restriction fragments of 12, 43, and 69 base pairs (Early et al., 1980b, 1981a,b). Analysis in those studies concentrated on R_2 and the initial values of R_1, and on the basis of those limited data, the results were interpreted to imply that the base pairs in the DNA wobbled about some average position as a result of wormlike motions. This resulted in effective corre-

lation times for reorientation of the base pairs that were shorter by a factor of 2–4 than the correlation times derived from hydrodynamic measurements (Early & Kearns, 1979; Early et al., 1981a). However, the present observations of the magnitude of R_1(long) demonstrate that even the slow, wormlike motions are inadequate to account for all the relaxation results and that relatively fast (0.5 ns) moderate amplitude (±30°) fluctuations in the base pair planes must be included. Several earlier studies of internal motions in DNA based on measurements of ^{31}P, ^{13}C, and ^{1}H relaxation indicate correlation times for internal motion of 0.2–5 ns (Bolton & James, 1979; Hogan & Jardetzky, 1980; Levy et al., 1981; Shindo, 1981; Keepers & James, 1982). However, with one exception (Hogan & Jardetzky, 1980), these previous studies monitored motions of the backbone. Hogan & Jardetzky's (1980) measurements of the C6 and C8 ^{13}C relaxation of calf thymus DNA directly bear on the motional properties of the base planes. They fit their data assuming a correlation time of 1×10^{-9} s and a fluctuation of ±20° in the orientation of the C–H bonds. Interestingly, the anisotropy of polarized fluorescence from ethidium bromide bound to DNA exhibits significant decay (from 0.4 to ~0.32) within a nanosecond, indicating substantial motion (~15°) of the base pair planes in relatively short times (Wahl et al., 1970; Millar et al., 1980; Thomas et al., 1980). The range of correlation times and fluctuation amplitudes determined from the NMR experiments may encompass both individual base pair motions and correlated bending and twisting motions such as those described by Barkley & Zimm (1979). It is evident, however, that the conformation of poly(dA-dT) is quite mobile, even on a 1-ns time scale.

Hydrogen-Bonding Geometry and Relaxation Rates. Relaxation of the longitudinal magnetization at low temperatures is primarily controlled by proton–proton dipolar interactions whereas the relaxation of the transverse magnetization contains a significant (40%) contribution from a dipolar interaction between the imino nitrogen and the imino proton. Since the N–H distance is expected to be only ~1.1 Å, the calculated value of R_2 is expected to be extremely sensitive to small (less than 0.1 Å) variations in $r_{N\text{-}H}$ but relatively less sensitive to interproton distances. Since J_0 terms dominate these two relaxation rates, comparing the ratio of $R_1(s)/R_2$ eliminates the necessity to calculate values for the spectral densities. In this way, the sensitivity of relaxation rates to choice of tumbling times and internal motion model is suppressed. If we use the interproton distances given in Table III then the experimental ratio of 5/1 for R_2/R_1 requires an N–H bond length of 1.14 ± 0.08 Å. This value may be compared with a value of 1.0 ± 0.1 Å previously obtained for A·T base pairs in restriction fragments using a more approximate analysis of the relaxation decay data. Di Verdi & Opella (1982) recently used solid-state NMR techniques and proton ^{15}N dipolar interactions to obtain a value of 1.13 Å (Di Verdi & Opella, 1982). X-ray diffraction studies (Hoogsteen, 1963) on model compounds yield values of 1.09, whereas neutron diffraction (Frey et al., 1973) yields a value of 1.04 Å. It appears that the relaxation method may be used to probe the hydrogen-bond geometry in DNA where applications of other techniques may be difficult, if not impossible.

Imino Proton Exchange Rates. Above 28 °C, the spin–lattice relaxation rate increases markedly with temperature, and the relaxation becomes exponential. This increase in the relaxation rate at high temperature is attributed to exchange of imino protons with bulk water protons as a result of transient opening and closing of base pairs in the duplex (Teitelbaum & Englander, 1975a). Analysis of the high-temperature relaxation data yields an activation energy of 17 ± 2 kcal/mol and a rate of ~5 s^{-1} at 300 K. It is interesting to compare these results obtained with poly(dA-dT) with results previously obtained by Teitelbaum and Englander for poly(A)·poly(U) (Teitelbaum & Englander, 1975a; Mandal et al., 1979) and by Early et al. (1980a,b, 1981a,b) for various DNA restriction fragments (Table VI). Within experimental error, and neglecting end effects present in the short restriction fragments, the activation energy for exchange of imino protons in A·U and A·T base pairs is found to be the same, independent of the system, sequence, and length. In particular, exchange rates measured in poly(dA-dT) are within a factor of 2, the same as those measured for A·T base pairs in restriction fragments located next to A·T base pairs, as well as to those that are sandwiched between two G-C base pairs that remain closed for much longer periods of time. These observations strongly support an exchange-out mechanism of A·T base pairs in those restriction fragments involving the opening of *individual* A·T base pairs with an apparent activation energy of ~16 kcal/mol and rate constant of 6 s^{-1} at 300 K.

It was recently proposed that the exchange behavior of poly(A)·poly(U) could be understood in terms of a mechanism in which "melted" open regions of base pairs propagate up and down the helix as a soliton (Englander et al., 1980; Krumhansl & Alexander, 1983). Since poly(dA-dT) has the same hydrogen bonding and similar exchange rates, the same mechanism should equally apply to this system. However, we have been able to demonstrate in DNA restriction fragments that G·C base pairs surrounding A·T base pairs remain closed even though the A·T base pair exchanges its imino proton with approximately the same rate as poly(dA-dT) (Early et al.,

Table VI: Thymine (Uracil) Imino Proton Exchange Rate Parameters in Various Polynucleotides

sample	τ_{ex}^{-1} (s^{-1}) (38 °C)	E_{act} (kcal/mol)
poly(rA)·poly(rU) (Mandal et al., 1979)	6.0	15 ± 0.9
random DNA, restriction fragments 12, 43, and 69 bp[a] (Early et al., 1981)	15–20	15.7
poly[d(AT)], 53 bp	12	17 ± 2

[a] bp = base pairs.

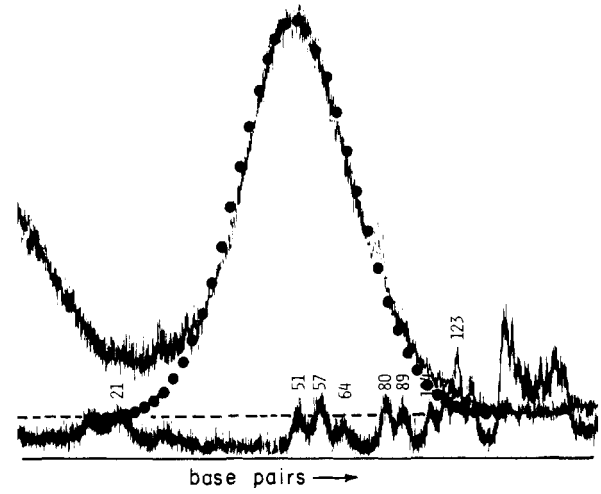

FIGURE 8: Comparison of the gel electrophoresis of sonicated poly(dA-dT) with pBR322 restriction fragments (see text). The circles (●) represent the calculated size distribution used in the heterogeneity calculation described in Appendix B.

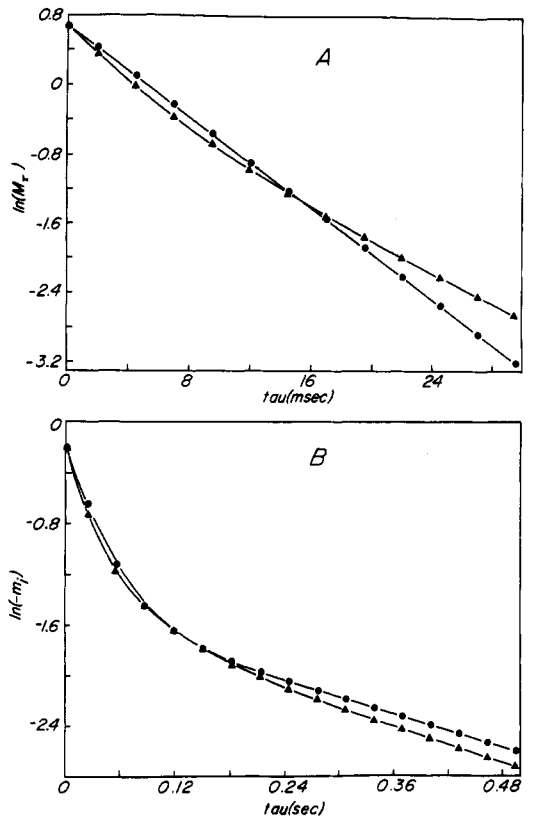

FIGURE 9: Comparison of (A) spin–spin and (B) spin–lattice relaxation curves calculated for a 53 base pair helix (●) with the curve calculated for the entire distribution of sizes shown in Figure 8 (▲).

1980b, 1981b). It is, therefore, difficult to see how soliton propagation could persist in the heterogeneous DNAs. Moreover, one might have expected to observe significant length effects, since the size of the open region is suggested to be on the order of 10 base pairs. Experimentally, little sequence or length effect on the exchange behavior is found. These results do not support the proposed soliton model, and we conclude that the new data obtained on poly(dA-dT) support the single-base opening model previously proposed by Mandal et al. (1979) and Teitelbaum & Englander (1975a,b) and reiterated by Early et al. (1980a,b, 1981b).

Acknowledgments

We thank Dr. Susan Amara and Summa Datta for their help in sizing the poly(dA-dT) samples, Dr. Peter A. Mirau for helpful discussions, and Dr. John M. Wright for his invaluable technical assistance.

Appendix

(A) Analysis of the Slow Spin–Lattice Relaxation Rates in DNA. Examination of the proposed X-ray structures of poly(dA-dT) reveals that some of the sugar protons are sufficiently close to provide a relaxation sink for the island of four spins (TNH, A-NH_2, and AH2) after initial equalization of the magnetization among these four spins. Most importantly, transfer of magnetization from the four-spin island to the nonexchangeable sugar protons occurs by zero-quantum (J_0) processes since m_s is initially zero for the nonexchangeable protons; however, the actual rate of magnetization transfer from spins in the island to the nonexchangeable protons will be relatively slow due to the large (>3 Å) distances involved. Relaxation involving nonexchangeable protons remains a zero-quantum process throughout most of the imino relaxation because the 19 tightly coupled nonexchangeable protons (per four-spin island) form such a large reservoir for the imino proton magnetization. Therefore, $|m_{\text{4-spin island}}| \gg |m_{\text{nonexchangeable}}|$ throughout the decay.

This analysis indicates that the observed relaxation of the imino proton at long times after a selective excitation of the imino proton (when magnetization is equalized among the protons in the four-spin island) consists of two major contributions: transfer of magnetization from the four-spin island to the lattice (via one- and two-quantum transitions) and transfer to the nonexchangeable protons (via zero-quantum transitions). Since the observed imino proton relaxation rate of 2.4 s^{-1} is an average relaxation rate of the four spins in the island, the total relaxation rate for the island is 4 times the observed rate, or 9.6 s^{-1}. We must now determine the contribution to this rate from each of the pathways mentioned above.

To separate the contributions of relaxation to the lattice and relaxation to the nonexchangeable protons, the results of the selective and nonselective relaxation experiments must be considered together. In the nonselective experiment, the observed imino proton relaxation rate is an average for 23 spins that behave as two separate islands of 4 and 19 spins, connected to one another by a slow transfer of magnetization. The connection is strongest when $m_{\text{nonexchangeable}}$ equals zero and zero when $m_{\text{4-spin island}} = m_{\text{nonexchangeable}}$. The interaction between these two islands is similar to the case of two spins weakly coupled by dipolar interactions and means that the observed nonselective relaxation rate will be affected by the magnetization of spins in the other island.

This model was evaluated by using a kinetic analysis to calculate the expected nonselective relaxation rate of the imino proton when the 4-spin imino island and the 19-spin island of nonexchangeable protons are all saturated. A nonselective relaxation rate of 0.5 s^{-1}, measured at 1 °C and 360 MHz for the nonexchangeable protons in D_2O (data not shown), was used as the average rate of relaxation to the lattice for each of the 19 spins in the nonexchangeable island. The rate of magnetization transfer from the 4-spin island to the 19-spin island is unknown, as is the rate of transfer of magnetization from the 4-spin island to the lattice. However, the total relaxation rate due to these two processes must be 9.6 s^{-1} to account for the observed imino behavior at long times after a selective excitation. A series of kinetic calculations were carried out in which the transfer of magnetization from the four-spin island to the lattice and to the nonexchangeable protons was varied but the total relaxation rate was fixed at 9.6 s^{-1}. These calculations resulted in nonselective relaxation rates for the imino proton ranging from 2.4 s^{-1} when all the relaxation was directly to the lattice to a rate of ~0.5 s^{-1} when all relaxation was with the 19 nonexchangeable protons. The calculated imino relaxation curves that fit the observed nonselective relaxation data are shown by the dashed lines in Figure 6A. These curves represent cases where the relaxation rate of the four-spin island to the lattice ranges from 8.0 to 5.6 s^{-1} and the relaxation rate with the nonexchangeable protons ranges from 1.6 to 4.0 s^{-1}. The average of this range is a rate of 2.8 ± 1.2 s^{-1} to the nonexchangeable protons and a relaxation rate of 6.8 ± 1.2 s^{-1} to the lattice. The nonselective relaxation rate of the imino proton with the lattice is expected to be one-fourth the rate observed for the four-spin island, i.e., 1.7 ± 0.3 s^{-1}.

If the imino proton is selectively excited, it relaxes rapidly with the neighboring protons with $R_1(\text{sel}) = 28$ s^{-1}. Thus, the magnetization received from the the excitation pulse is rapidly equilibrated among the four protons in the imino island.

Relaxation continues from these four spins to the lattice and also through weak connections with the nonexchangeable protons surrounding the four-spin island. The rate of transfer of magnetization from the four-spin island to the nonexchangeable protons is roughly 2.8 ± 1.2 s^{-1}, and relaxation with the lattice is approximately 6.8 ± 1.2 s^{-1}. Thus, the observed relaxation rate at long times after the selective excitation of the imino proton is (6.8 ± 2.8) $s^{-1}/4$ = 2.4 s^{-1}.

(B) Effect of Size Heterogeneity on Relaxation Rates of DNA. Short pieces of DNA for NMR studies are usually prepared by some method of cutting or shearing large DNA. These methods invariably produce DNA fragments with a distribution of sizes even after narrowing by purification procedures, but for purposes of analysis these samples are usually treated as though they were homogeneous. The current analysis provides us the opportunity to test the validity of this assumption.

The densitometer tracing of a photograph taken of a sizing gel run on the poly(dA-dT) and pBR322 restriction fragments (see Materials and Methods) is shown in Figure 8. To test the assumption that the NMR relaxation of DNA with this size distribution can be accurately analyzed as if all molecules were 53 base pairs long, a size distribution was generated to match the observed distribution. The observed distribution was accurately fit with the function $Y = A \exp[-B(\Delta X)^2]$ where ΔX = [ln (number of base pairs) − ln (53 base pairs)] and $B = 5.67$. The calculated distribution is represented by the circles in Figure 9.

R_1(sel), R_1(long), and R_2 were then calculated assuming ±30° of internal motion and a correlation time of 0.6 ns for each DNA fragment size present in the distribution. These rates were then used in the kinetic analysis to generate the expected relaxation curve for each DNA fragment. The resulting relaxation curves were weighted proportionally to the relative number of that sized fragment in the distribution and averaged. The relaxation curves calculated in this manner are compared with the results calculated assuming a homogeneous size of 53 base pairs in Figure 9. In the case of spin–spin relaxation, the curves are similar at short times, but the curve calculated for the average deviates somewhat at long times. However, due to scatter in the data points at long times, we are unable to distinguish between these two curves. For spin–lattice relaxation, the two curves are virtually identical. The close matches between the relaxation curves for the homogeneous and averaged relaxation curves in both cases indicate that it is valid to treat this DNA size distribution as though all of the molecules were of one length. A similar calculation performed assuming that the DNA behaved as a rigid rod produced curves so far from the observed curves that we do not bother to show them here. This analysis should alleviate any concern that the observed nonexponential longitudinal relaxation is due to a distribution of DNA lengths in the sample.

Registry No. Poly(dA-dT), 26966-61-0; hydrogen, 1333-74-0.

References

Abragam, A. (1961) in *The Principles of Nuclear Magnetism* (Marshall, W. C., & Wilkinson, D. H., Eds.) Clarendon Press, Oxford, England.

Anderson, S., Bankier, A. T., Barrell, B. G., de Bruijn, M. H. L., Coulson, A. R., Drouin, J., Eperon, I. C., Nierlich, D. P., Roe, B. A., Sanger, F., Schreier, P. H., Smith, A. J. H., Staden, R., & Young, I. G. (1981) *Nature (London) 290*, 457.

Arnott, S., Chandrasekaran, R., Hukins, D. W. L., Smith, P. J. C., & Watts, L. (1974) *J. Mol. Biol. 88*, 523.

Arnott, S., Chandrasekaran, R., Puigianer, L. C., Walker, J. K., Hall, I. H., Birdsall, D. L., & Ratliff, R. L. (1983) *Nucleic Acids Res. 11*, 1457.

Baldwin, R. L. (1971) *Acc. Chem. Res. 4*, 265.

Barkley, M. D., & Zimm, B. H. (1979) *J. Chem. Phys. 70*, 2991.

Bolton, P. H., & James, T. L. (1979) *J. Phys. Chem. 83*, 3359.

Brahms, S., Brahms, J., & Van Holde, K. E. (1976) *Proc. Natl. Acad. Sci. U.S.A. 73*, 3453.

Broersma, S. (1960) *J. Chem. Phys. 32*, 1626.

Charney, E., & Yamaoka, K. (1982) *Biochemistry 21*, 834.

Dickerson, R. E., Kopka, M. L., & Drew, H. R. (1982) in *Conformation in Biology* (Srinivasan, R., & Sarma, R. H., Eds.) p 227, Adenine Press, New York.

Di Verdi, J. A., & Opella, S. J. (1982) *J. Am. Chem. Soc. 104*, 1761.

Drew, H. R., & Dickerson, R. E. (1982) *EMBO J. 1*, 663.

Drew, H. R., Wing, R. M., Takano, T., Broka, C., Tanaka, S., Itakura, K., & Dickerson, R. E. (1981) *Proc. Natl. Acad. Sci. U.S.A. 78*, 2179.

Early, T. A., & Kearns, D. R. (1979) *Proc. Natl. Acad. Sci. U.S.A. 76*, 4165.

Early, T. A., Feigon, J., & Kearns, D. R. (1980a) *J. Magn. Reson. 41*, 343.

Early, T. A., Kearns, D. R., Hillen, W., & Wells, R. D. (1980b) *Nucleic Acids Res. 8*, 5795.

Early, T. A., Kearns, D. R., Hillen, W., & Wells, R. D. (1981a) *Biochemistry 20*, 3756.

Early, T. A., Kearns, D. R., Hillen, W., & Wells, R. D. (1981b) *Biochemistry 20*, 3764.

Englander, S. W., Kallenbach, N. R., Heeger, A. J., Krumhansl, J. A., & Litwin, S. (1980) *Proc. Natl. Acad. Sci. U.S.A. 77*, 7222.

Fratini, A. V., Kopka, M. L., Drew, H. R., & Dickerson, R. E. (1982) *J. Biol. Chem. 257*, 14686.

Frey, M. M., Koetzke, T. F., Lehmann, M. S., & Hamilton, W. C. (1973) *J. Chem. Phys. 59*, 915.

Granot, J., Assa-Munt, N., & Kearns, D. R. (1982) *Biopolymers 21*, 873.

Greve, J., Maestre, M. F., & Levin, A. (1977) *Biopolymers 16*, 1489.

Hagerman, P. J. (1981) *Biopolymers 20*, 1503.

Hahn, E. L. (1950) *Phys. Rev. 80*, 580.

Hogan, M. E., & Jardetzky, O. (1980) *Biochemistry 19*, 3460.

Hoogsteen, K. (1963) *Acta Crystallogr. 16*, 28.

Kalk, A., & Berendsen, H. J. C. (1976) *J. Magn. Reson. 24*, 343.

Kearns, D. R. (1984) *CRC Crit. Rev. Biochem.* (in press).

Kearns, D. R., Assa-Munt, N., Behling, R. W., Early, T. A., Feigon, J., Granot, J., Hillen, W., & Wells, R. D. (1981) in *Proceedings of the Second SUNYA Conversation in the Discipline Biomolecular Stereodynamics* (Sarma, R. H., Ed.) Vol. I, p 345, Adenine Press, New York.

Kearns, D. R., Assa-Munt, N., Behling, R., Denny, W. A., Feigon, J., Granot, J., Leupin, W., & Mirau, P. (1983) *Biophys. J. 41*, 210a.

Keepers, J. W., & James, T. L. (1982) *J. Am. Chem. Soc. 104*, 929.

Klug, A., Jack, A., Viswamitra, M. A., Kennard, O., Shakked, Z., & Steitz, T. A. (1979) *J. Mol. Biol. 131*, 669.

Krumhansl, J. A., & Alexander, D. M. (1983) in *Structure and Dynamics: Nucleic Acids and Proteins* (Clementi, E., & Sarma, R. H., Eds.) p 61, Adenine Press, New York.

Levy, G. C., Hilliard, P. R., Jr., Levy, L. F., & Rill, R. L. (1981) *J. Biol. Chem. 256*, 9986.

Lipari, G., & Szabo, A. (1982) *J. Am. Chem. Soc. 104*, 4546, 4559.
Mahendrasingam, A., Rhodes, N. J., Goodwin, D. C., Nave, C., Pigram, W. J., Fuller, W., Brahms, J., & Vergne, J. (1983) *Nature (London) 301*, 535.
Mandal, C., Kallenbach, N. R., & Englander, S. W. (1979) *J. Mol. Biol. 135*, 391.
Marky, L. A., Patel, D., & Breslauer, K. J. (1981) *Biochemistry 20*, 1427.
McKnight, S. L., & Kingsbury, R. (1982) *Science (Washington, D.C.) 217*, 316.
Millar, D. P., Robbins, R. J., & Zewail, A. H. (1980) *Proc. Natl. Acad. Sci. U.S.A. 77*, 5593.
Mirau, P. A., & Kearns, D. R. (1983) in *Structure and Dynamics: Nucleic Acids and Proteins* (Clementi, E., & Sarma, R. H., Eds.) p 227, Adenine Press, New York.
Moreau, J., Marcaud, L., Maschat, F., Kejzlarova-Lepesant, J., Lepesant, J.-A., & Scherrer, K. (1982) *Nature (London) 295*, 260.
Noggle, J. H., & Schirmer, R. E. (1971) in *The Nuclear Overhauser Effect*, p 1, Academic Press, New York.
Patel, D. J. (1978) *J. Polym. Sci., Polym. Symp. 62*, 117.
Patel, D. J., & Canuel, L. (1976) *Proc. Natl. Acad. Sci. U.S.A. 73*, 674.
Patel, D. J., & Canuel, L. L. (1977) *Biopolymers 16*, 857.
Radwan, M. M., & Wilson, H. R. (1982) *Int. J. Biol. Macromol. 4*, 145.
Reddy, V. B., Thimmappaya, B., Dhar, R., Subramanian, K. N., Zain, B. S., Pan, J., Ghosh, P. K., Celma, M. L., & Weissman, S. M. (1978) *Science (Washington, D.C.) 200*, 494.
Redfield, A. G., & Kunz, S. D. (1979) in *NMR and Biochemistry* (Opella, S. J., & Lu, P., Eds.) p 225, Marcel Dekker, New York.
Shindo, H. (1981) *Eur. J. Biochem. 120*, 309.
Teitelbaum, H., & Englander, S. W. (1975a) *J. Mol. Biol. 92*, 55.
Teitelbaum, H., & Englander, S. W. (1975b) *J. Mol. Biol. 92*, 79.
Thomas, J. C., Allison, S. A., Appelof, C. J., & Schurr, J. M. (1980) *Biophys. Chem. 12*, 177.
Viswamitra, M. A., Shakked, Z., Jones, P. G., Sheldrick, G. M., Salisbury, S. A., & Kennard, O. (1982) *Biopolymers 21*, 513.
Vorlickova, M., Kypr, J., Kleinwachter, V., & Palecek, E. (1980) *Nucleic Acids Res. 8*, 3965.
Wagner, G., & Wüthrich, K. (1979) *J. Magn. Reson. 33*, 675.
Wahl, P., Paoletti, J., & Le Pecq, J.-B. (1970) *Proc. Natl. Acad. Sci. U.S.A. 65*, 417.
Wang, A. H.-J., Quigley, G. J., Kolpak, F. J., Crawford, J. L., van Boom, J. H., van der Marel, G., & Rich, A. (1979) *Nature (London) 282*, 680.
Woessner, D. E. (1962) *J. Chem. Phys. 37*, 647.
Woessner, D. E., Snowden, B. S., Jr., & Meyer, G. H. (1969) *J. Chem. Phys. 50*, 719.
Wright, J. M., Feigon, J., Denny, W., Leupin, W., & Kearns, D. R. (1981) *J. Magn. Reson. 45*, 514.

Arsenic Mononucleotides. Separation by High-Performance Liquid Chromatography and Identification with Myokinase and Adenylate Deaminase†

Rosario Lagunas,* David Pestaña, and José C. Diez-Masa

ABSTRACT: The spontaneous formation of arsenic mononucleotides has been detected in mixtures of arsenate and inosine or adenosine or its deoxy analogues. These compounds have been separated by high-performance liquid chromatography and identified by their behavior in the presence of myokinase and adenylate deaminase. The nucleoside 5′-arsenates are formed preferentially to the 2′- and 3′-arsenate analogues. All arsenic nucleotides detected showed similar kinetic and equilibrium constants of formation: about 8×10^{-4} M^{-1} s^{-1} and 2×10^{-3} M^{-1}, respectively. These values are several orders of magnitude greater than those of their phosphoric analogues. The adenosine 5′-arsenate was able to substitute for 5′AMP in the reaction of myokinase and adenylate deaminase. The substitutions of the 2′- or 3′-hydrogen for hydroxyl groups in the ribose moiety of this compound slightly affected its suitability as substrate for myokinase but had drastic effect in the case of adenylate deaminase. The half-life of the arsenic nucleotides, at pH 7.0 and 25 °C, ranged from 30 to 45 min. The lability of these compounds is increased during catalysis with myokinase. Results on the reaction mechanism of myokinase with adenosine 5′-arsenate indicate that the mixed-anhydride analogue to ADP, adenosine 5′-(arsenate phosphate), is not detected either because it is not formed in the reaction with this enzyme or because it is rapidly hydrolyzed.

The occurrence of labile arsenic esters in cells supplied with arsenate was postulated (Braunstein, 1931) to explain the observation that arsenate decreased alcoholic fermentation in yeast (Harden & Young, 1906). Evidence supporting this hypothesis was obtained when the existence of sugar–arsenic esters was demonstrated in mixtures of sugars and arsenate (Lagunas, 1968; Long & Ray, 1973; Lagunas, 1980). The formation of arsenic nucleotides has been the subject of intensive investigation in mitochondria because the uncoupling effect of arsenate on the oxidative phosphorylation was explained through the formation of a labile intermediate of this type (Ernster el al., 1967; Bertagnolli & Hanson, 1973). However, although some evidence was reported for the oc-

† From the Instituto de Enzimología y Patología Molecular del CSIC, Facultad de Medicina de la UAM, Madrid-34, Spain, and the Instituto de Química Orgánica del CSIC, Juan de la Cierva 3, Madrid-6, Spain. *Received July 8, 1983.* Supported by Fondo Nacional para la Investigación Científica y Técnica.

0006-2960/84/0423-0955$01.50/0